21st century changes in snow water equivalent over Northern Hemisphere landmasses due to increasing temperature, projected with the CMIP5 models

By

H. X. Shi and C. H. Wang

Key Laboratory of Arid Climate Change and Disaster Reduction of Gansu Province,

College of Atmosphere Science, Lanzhou University, Lanzhou, China, 730000

Abstract. Changes in snow water equivalent (SWE) over Northern Hemisphere (NH) landmasses are investigated for the early (2016−2035), middle (2046−2065) and late (2080−2099) 21st century using 20 global climate models from the Coupled Model Intercomparison Project Phase 5 (CMIP5). The multi-model ensemble projects a significant decrease in SWE for most regions relative to the 1986–2005 mean under three Representative Concentration Pathways (RCP). This decrease is particularly evident over the Tibetan Plateau and western North America, whereas an increase occurs over eastern Siberia. Seasonal SWE projections show an overall decreasing trend, with the greatest reduction in spring, this is linked to the stronger inverse partial correlation between SWE and increasing temperature. The largest relative

reduction in SWE over the NH does not occur in spring but in summer. Zonal mean annual SWE exhibits significant reductions for three RCPs, and the magnitude of the reduction gradually decreases with latitude in the NH from south to north. A strong linear relationship between SWE and temperature at mid–high latitudes suggests that the reduction in SWE in this region is related to rising temperature. As temperature increases, the reduction in the fraction of solid precipitation becomes the main contributor to the change in SWE from August to May in the next year in the 21st century, and after May the reduction in SWE is controlled primarily by the decrease in accumulated snowfall. In summary, our results show a trend towards decreasing SWE, and the decreases in solid precipitation and accumulated snowfall strongly affect the change in SWE before and after May, respectively.

Key words: Coupled Model Intercomparison Project (CMIP5); Snow water equivalent (SWE); Model assessment and projection; Sensitivity

1 Introduction

Snow is a key component of the cryosphere and plays a fundamental role in global climate due to its high albedo and cooling effect (Vavrus, 2007). However, terrestrial snow cover in the Northern Hemisphere (NH) is changing rapidly alongside increasing global temperatures. According to the IPCC Fifth Assessment Report (AR5) (IPCC, 2013) NH snow cover extent decreased by 1.6 [0.8 to 2.4]% per decade for March and April, and by 11.7 [8.8 to 14.6]% per decade for June, during the period 1967–2012. Furthermore, the projections show a 7% decrease in the total area of NH spring snow cover for Representative Concentration Pathway (RCP) 2.6 and a 25% decrease for RCP8.5 by the end of the 21st century. This result is consistent with results from the IPCC Fourth Assessment Report (AR4) (IPCC, 2007). Projections of mean annual NH snow cover suggest a further 13% reduction by the end of the 21st century under the B2 scenario, with individual projections ranging from 9% to 17%; i.e., despite different emission scenarios, the change in snow cover over the NH land shows the same decreasing trend.

Several studies have shown that marked decreases in the area and/or depth of snow have already occurred in regions such as western North America (Groisman et al., 2004; Stewart et al., 2005), central Europe (Falarz, 2002; Vojtek et al., 2003; Scherrer et al., 2004) and China (Ji et al., 2012; Wang et al., 2012), thus highlighting the need for better projections of future snow conditions.

Snow cover represents a spatially and temporally integrated response to snowfall events (Brown and Mote, 2009), and may have a direct relationship with temperature (Brutel-Vuilmet et al., 2013). Snow depth mainly reflects the magnitude of precipitation (snowfall), whereas snow water equivalent (SWE) primarily reflects the combined impact of temperature and precipitation (Räisänen, 2008). According to AR5 (IPCC, 2013), global temperature and precipitation will increase in the 21st century. The dependence of global

warming on the RCP emission pathway is weak for the next few decades but strengthens rapidly towards the end of this century (IPCC, 2013). Of primary concern is the way that SWE will respond to changes in temperature and precipitation. AR5 reported that SWE responds to both temperature and precipitation, and is more sensitive to the snowfall amount at the beginning and end of the snow season (IPCC, 2013).

Global climate models consistently project declining SWE in many areas by the end of the 21st century, while some models show an increase in snowpack along the Arctic Rim by 2100 (Hayhoe et al., 2004; Brown and Mote, 2009). For example, a 20-km-mesh atmospheric general circulation model projects decreased SWE over much of the NH, and increased SWE over cold regions (Siberia and northernmost North America) due to increasing snowfall during the coldest months (Hosaka et al., 2005). Brutel-Vuilmet et al. (2013) also indicated that the greatest relative reduction in maximum SWE at low latitudes is related to decreasing snowfall.

Räisänen (2008) suggested that changes in seasonal SWE by the end of the 21st century will vary regionally and depend on local climate conditions. In very cold regions, for example, warming will result in increased winter snowfall, and thus a thicker snowpack, whereas in warm regions the higher temperatures will result in decreased snowfall. Similarly, CMIP5 experiments project declining SWE over North America south of 70°N (concentrated over the Rocky Mountains, southern Alaska and the eastern Canadian provinces), with maximum changes during the peak snow season (January−April), and increasing SWE north of 70°N due to enhanced precipitation (Maloney et al., 2012). In the mountainous regions of Europe and western North America, projected reductions in SWE are greatest at low elevations (Maloney et al., 2012). SWE is generally projected to decrease less with increasing altitude due to colder winter conditions, but in some areas simulated SWE actually increases with altitude (Scherrer et al., 2004; Mote et al., 2005; Mote, 2006).

According to AR5 (IPCC, 2013), anthropogenic warming will continue

beyond 2100 for all RCPs, leading to an acceleration of the water cycle and a changing ratio of snowfall to rainfall. Moreover, increased winter precipitation will likely be insufficient to offset the greater contribution of liquid precipitation and enhanced snowmelt driven by higher average temperatures (Räisänen and Eklund, 2011). From TAR to AR5, projected linear trends in SWE under different scenarios are highly variable since SWE is dependent both on the concentration of total emissions and the duration of emissions.

The above studies show that changes in SWE generally depend on both temperature and precipitation, but their relative contributions remain debated. Several studies have concluded that increasing temperature plays a major role in decreasing SWE (Lemke et al., 2007; Räisänen and Eklund, 2011), whereas other studies indicate that increasing SWE is mainly related to increasing precipitation (Hosaka et al., 2005; Maloney et al., 2012). Räisänen (2008) suggested that changes in SWE depend on the competing influences of temperature and precipitation; i.e., an increase in precipitation, if acting alone, would lead to an increase in snowfall and consequently to increased amounts of snow on ground, while an increase in temperature alone would reduce the fraction of precipitation that falls as snow and increase snow melt. Consequently, the present study was motivated by the need to address the following questions: (1) How will NH SWE respond to different RCPs in the 21st century? (2) How will the relationships between SWE and temperature, and between SWE and precipitation change during different periods of the 21st century?

To further analyze anticipated changes in SWE, we employed outputs from the CMIP5 models in conjunction with the GlobSnow product. We focus primarily on temporal and spatial changes in SWE and on variations in the relationship between SWE and climate for each RCP during different periods of the 21st century. The specific datasets used in this study are described in Section 2, and the simulated and observed data are compared in Section 3. The temporal and spatial characteristics of SWE projections are analyzed in

Section 4, and the relationships between SWE and climate change are discussed in Section 5. Finally, the key findings of the study are summarized in Section 6.

2 Datasets

To objectively quantify the changes in SWE in the 21st century, we examined 20 models participating in CMIP5 (Table 1). These models all provide monthly SWE in historical experiments and three scenario experiments (RCP2.6, RCP4.5 and RCP8.5), and we only use the first ensemble member produced by each model (e.g., r1i1p1). While these models vary in their forcing parameters, each model includes an increase in major anthropogenic aerosols observed during 1850–2005 and anticipated for future scenarios. Further details can be found at http://www-pcmdi.llnl.gov.

The model simulations cover the periods 2006−2099 and 2006−2300. Here, we describe changes in SWE during the former period, which is divided into three sub-periods: the early (2016−2035; EP), middle (2045−2065; MP) and late (2080−2099; LP) 21st century. The analyses were conducted using a 1° × 1° latitude–longitude grid, and re-gridding of original model grids was conducted via bilinear interpolation.

To verify the performance of the CMIP5 models for simulating SWE, we compare the CMIP5 outputs with monthly SWE data from the European Space Agency (ESA) GlobSnow dataset (Takala et al., 2011). GlobSnow combines SWE retrieved from passive microwave and weather station observations. This is the most realistic SWE product currently available (Hancock et al., 2013) because of the improved accuracy achieved by assimilating independent sources of information. The series covers the period 1979–2010 with a resolution of 25 × 25 km, and is also interpolated onto a common 1° × 1° grid. Hereafter, we refer to the GlobSnow dataset as the observed SWE.

In this paper, linear correlation coefficients, partial correlation analysis and regression analysis are used to investigate the relation between model

simulations from different scenario experiments and observations. The equations are as follows.

Partial correlation:

$$r_{XY,Z} = \frac{r_{XY} - r_{XZ} r_{YZ}}{\sqrt{(1 - r_{XZ}^2)(1 - r_{YZ}^2)}} \quad (1)$$

where $r_{XY,Z}$ indicates the contribution of *X* to *Y*, after removing the contribution of *Z* to *Y*.

Regression coefficient:

$$Y = b + at \quad (2)$$

where *a* represents the linear trend of factor *Y* with time *t*.

Relative-error ratio (RE):

$$RE = \frac{S_i - O_i}{O_i} \times 100\% \quad (3)$$

where *RE* reflects the change in a variable *S* relative to the baseline *O*.

Räisänen (2008) suggested that the change in SWE (ΔSWE) can be decomposed into four terms:

$$\Delta SWE = \underbrace{\overline{G}\int \overline{F}\Delta P dt}_{\Delta SWE(\Delta P)} + \underbrace{\overline{G}\int \Delta F\,\overline{P} dt}_{\Delta SWE(\Delta F)} + \underbrace{\Delta G\int \overline{F}\,\overline{P} dt}_{\Delta SWE(\Delta G)} + \underbrace{\frac{1}{4}\Delta G\int \Delta F \Delta P dt}_{\Delta SWE(NL)} \quad (4)$$

where the first three terms on the right represent the contribution from changes in total precipitation (ΔP), fraction of solid precipitation (ΔF) and the fraction of accumulated snowfall that remains on the ground (ΔG). $\Delta SWE(NL)$ is a non-linear combination of ΔG, ΔF and ΔP. P_1 is mean total precipitation during different periods of the 21st century, and P_0 is the mean total precipitation during 1986–2005. $\overline{P} = (P_0 + P_1)/2$, $\Delta P = (P_1 - P_0)$, the definitions of $\overline{G}, \Delta G, \overline{F}, \Delta F$ can refer to $\overline{P}, \Delta P$.

3 Validation of CMIP5 SWE simulations

To evaluate the simulation performance of the models used in this study, we calculated spatial correlations and standard deviation ratios for the observed and simulated winter (DJF) mean SWE (Figure 1). Simulated SWE from each model exhibits a strong spatial correlation ($p < 0.05$) with observations, and most standard deviation ratios (i.e., model to observation) are close to one. These results indicate that the models can reproduce the spatial characteristics of SWE. Furthermore, the multi-model ensemble can improve simulation performance, and has better correlation and standard deviation ratios than most individual models. Figure 2 shows both the observed and simulated mean winter SWE over NH land covered by the GlobSnow data. The observed mean winter SWE over the NH is 71.6 kg m^{-2}, while the simulation ranges from 61.0 to 111.3 kg m^{-2}. The RE ranges from −20.3% to 55.4%. Most models overestimate SWE, and only five models (CanESM2, CSIRO-Mk3-6-0, HadGEM2-ES, MPI-ESM-LR and MPI-ESM-MR) underestimate SWE, with a RE of −20% to −0.4%. However, the multi-model mean is 80.8 kg m^{-2}, which is closer to observation than most of the individual models. This illustrates that the multi-model ensemble is more effective for simulating changes in SWE than individual models. From here on, all reported simulation values are from the multi-model ensemble mean, and we take the period 1986–2005 from the historical experiment (1850–2005) as the reference period.

4 Changes in SWE in the 21st century

To project future spatial and temporal SWE patterns, we analyze three RCP simulations (RCP2.6, RCP4.5 and RCP8.5).

4.1 Spatial changes in SWE for three RCPs

Projected spatial changes in SWE relative to 1986–2005 (RP) for three periods of the 21st century are shown in Figure 3. The mean annual SWE declines over much of the NH for all RCPs, with the greatest changes occurring over the Tibetan Plateau (TP); the multi-model mean decrease in SWE

exceeds 80% in the western TP. The only regions where a weak increase in SWE (RE < 20%) is observed are eastern Russia and Siberia. Over North America, north of 60°N, there is a pronounced reduction in SWE during the LP for RCP8.5 with an RE that ranges from −40% to −10%. For both RCP2.6 and RCP4.5 the RE ranges from −20% to −10%. In contrast, in eastern Siberia the RE is from 10% to 20% for RCP8.5, while for both RCP2.6 and RCP4.5 the RE is <10%. This distribution suggests that the magnitude of the SWE decrease (increase in Siberia) gradually becomes larger with time and with higher emissions.

The changes in SWE in winter and spring (not shown) show a similar pattern to that of mean annual SWE. In springtime, for example, the RE is between −20% and −10% over northern North America and ranges from −40% to −20% over most of Europe. In Siberia, the multi-model mean increase in SWE exceeds 10%. Over the whole NH, the extent of increased springtime SWE (RE > 0) is comparable to that in winter and for the annual mean. Nonetheless, the magnitude of the decline in spring SWE exceeds that in winter so that the decrease in SWE in spring is more significant than in winter.

As global temperatures rise, the projected reduction in SWE is most pronounced along the southern limits of seasonal snow cover. This is particularly apparent over the TP, a unique cold, high-altitude region (Figure 3) where the increase in temperature is more rapid than in other mid-latitude areas (Liu, 2000; Chen, 2006; Wang et al., 2012), atmospheric warming may accelerate snowmelt and result in reduced total snowfall amounts.

Figure 4 illustrates the relative zonal changes in mean annual SWE, precipitation and the absolute change in temperature derived from the multi-model mean for three periods of the 21st century. For all variables, the temporal trends in the multi-model mean are roughly similar in different RCPs during the same period. However, the magnitude of changes in mean annual SWE, precipitation and temperature increase with emissions (RCP) and with time.

The decrease in SWE is small in the 60–70°N latitude band for all three RCPs throughout the 21st century (RE < 30%), and the magnitude of decrease in SWE gradually declines from south to north (north of 60°N), namely, the largest relative reduction in SWE occurs at the low latitude. However, the largest absolute change in SWE (not shown) appears in the high latitudes (70−80°N). Relative to the RP, the magnitude of reduction in NH SWE gradually increases over time with increased emissions. During the LP, the absolute decrease in SWE reaches −28.0 kg m^{-2} for RCP2.6, −55.7 kg m^{-2} for RCP4.5 and −77.6 kg m^{-2} for RCP8.5.

Figure 4 d–f shows that temperature will increase more rapidly at high latitudes than at low latitudes. AR5 also shows that anthropogenic warming will be more pronounced at high latitudes (IPCC, 2013). The temperature increase is greater over time and with higher emissions (RCP), and temperature increases more rapidly in the 50–60°N latitude band than in other areas. The temperature increase does not exceed 2°C in RCP2.6 by the end of the 21st century, which is in agreement with the results of AR5 (IPCC, 2013). Similarly, a greater increase in precipitation occurs in tropical and high-latitude regions during the EP, MP and LP for all three RCPs (Figure 4g–i). The minimum increase in precipitation occurs in the 30–40°N latitude band, which is likely related to the fact that most arid regions in the NH are located in this region. During the EP, relative changes in precipitation are the same for all three RCPs, but these grow larger with time and increased emissions. During the LP, the increase in precipitation exceeds 30% for RCP8.5 at high-latitudes (70–80°N) whereas changes for the mid–low emission scenarios (RCP2.6, RCP4.5) are generally less than 20%.

The above results show that both the relative and absolute changes in SWE show a tendency to decline with time and with increased emissions. The most significant relative reduction in SWE occurs at low latitudes, where snow may gradually disappear with the temperature increasing in the 21st century. Another significant relative and absolute change in SWE occurs in the Arctic, where

significant temperature and precipitation increases are projected. This result indicates that decreasing SWE will likely lead to acceleration of the hydrologic cycle.

In general, precipitation increases will lead to an increase in SWE, however, at high latitudes SWE does not increase alongside increased precipitation in all RCPs and periods (Figure 4), which indicates that the decrease in SWE is governed by temperature. However, the Arctic (north of 70°N) is characterized by significant increases in temperature and precipitation, and a significant decrease in SWE. This result suggests that the fraction of accumulated snowfall that remains on the ground (snow cover) will decrease, and it reflects the non-linear relationships between temperature and precipitation and accumulated snowfall.

To analyze the relationships between the decrease in SWE and the increase in temperature, Table 2 shows slopes of the regression between projected interannual SWE and temperature, and the correlation coefficients for SWE and temperature at different latitude bands in the three RCPs. During the EP, linear relationships between SWE and temperature are significant in all latitude bands, which illustrates that SWE decreases alongside increasing temperature. There are also significant negative correlations between SWE and temperature; i.e., increasing temperature leads to decreasing SWE. However, for RCP2.6 this relationship is only observed in the EP, and not in the MP and LP except in the 40–50°N latitude band. Similarly, for RCP4.5 there is significant negative relationship between SWE and temperature in the EP. This relationship is observed north of 40°N in the MP, and gradually moves northward, only occurring in the 40–60°N latitude band in the LP. Of note, a significant negative relationship between SWE and temperature is observed in RCP8.5 during all three periods.

A comparison of Figure 4 with Table 2 shows that although temperature is a key factor in controlling SWE, the rate of the temperature increase is not the same as the rate of the SWE decrease. In other words, SWE decreases in

response to a specific temperatures range.

In AR4 (IPCC, 2007), temperatures in the 40−60°N latitude band were closely correlated with the area of springtime snow cover (r = −0.68). This correlation increased to −0.76 in AR5 (IPCC, 2013). The present results support these findings, suggesting that the most significant changes in SWE will occur at mid to high latitudes during winter and spring (not shown). Furthermore, the correlation between SWE and temperature during different periods of the 21st century is stronger, even more than that reported by AR5 (IPCC, 2013), indicating that SWE at mid to high latitudes will persistently decrease with rising temperatures.

4.2 Seasonal changes in SWE

Figure 5 shows the monthly variation in SWE and its relative change (RE) over NH land (excluding Greenland) during different periods of the 21st century. Multi-model ensemble simulations during the RP reproduce the basic features of the monthly variation in observed SWE (GlobSnow), with the maximum SWE in spring, and minimum SWE in summer (not shown). These same features are evident in simulations of the EP, MP and LP for the three different RCPs (Figure 5a-c), although the main difference is that total SWE throughout the 21st century is lower than during the RP.

Figure 5d–f shows changes (RE) in SWE during the EP, MP and LP for all three RCPs relative to the RP. For all three periods of the 21st century, the greatest decrease in SWE occurs during summer, while the smallest reduction occurs in spring. In the first 20 years of the 21st century, the change in SWE relative to the RP is the same in all three RCPs (Figure 5d), and differences among the RCPs are more evident during the MP and LP (Figure 5e–f). During the last period of the 21st century (LP), the maximum reduction in SWE is 66.4% for RCP8.5, and ranges from 27.5% for RCP2.6 to 39.8% for RCP4.5. In contrast, the largest absolute change in SWE appears in spring, with the smallest decline in summer. The relative change in SWE is thus predicted to be markedly different to the absolute change.

Temperature and precipitation are the dominant parameters influencing SWE, and both exhibit considerable changes in seasonality (Figure 6). Relative to the RP, temperatures are projected to rise during the EP (Figure 6a), MP (Figure 6c) and LP (Figure 6e) for all three RCPs, with the greatest warming occurring in winter and the smallest in summer. The magnitude of the temperature change increases with higher emissions over time. In the EP, the temperature increase does not exceed 2°C for all three RCPs, and larger differences emerge during the MP and LP. Moreover, a basic feature is that the temperature increase is significant in the tropics and Arctic regions during the three periods of 21st century.

Precipitation also increases throughout the 21st century for all three RCPs (Figure 6d–f), and changes in precipitation during winter exceed those during summer, despite the larger absolute change in precipitation in summer. During the EP, the magnitude of precipitation increase is the same for all three RCPs, and the change gradually grows larger with increased emissions over time. A noticeable feature of the model outputs is that changes in precipitation for mid–low emissions are not significant during the MP and LP, the largest increase in precipitation occurs during winter in the LP for RCP8.5, and the RE exceeds 20%.

SWE tends to decrease alongside the increase in global temperature throughout the 21st century. To further validate this finding for SWE in different RCPs, Table 2 shows the regression slope for mean annual SWE and mean temperature over different latitude bands in the NH during the RP, EP, MP and LP. The results show a significant decrease in SWE for RCP8.5 during the EP, MP and LP. However, for the mid–low emission scenario, a significant decrease in SWE at different latitude bands only occurs persistently in the EP. In the MP and LP, a significant decrease in SWE occurs mainly in the mid–high latitude band. The distribution in the linear trend of mean annual SWE (not shown) shows decreases over northern North America and the TP, and increases over Siberia. This pattern indicates that the change in mean annual SWE is spatially

variable, which is consistent with the spatial change shown in Figure 3.

On a seasonal scale, the extent and magnitude of the SWE increase in winter is larger than in spring, but the range and magnitude of the SWE decrease is significantly smaller than in spring. This is due to the later shift from liquid to solid precipitation in autumn and an earlier onset of snowmelt in spring (Räisänen, 2008). Consequently, the reduction in SWE averaged over the NH is more significant in spring than in winter.

There is high model uncertainty of SWE simulation in the 21st century, especially for RCP8.5, this is illustrated in Figure 7, which also shows the range of uncertainty in the mid–low emission scenario. However, despite model uncertainty, annual SWE still exhibits a consistent and significant decline for each of the three RCPs, with a linear trend of −0.54 kg m^{-2}/10a for RCP2.6, −1.09 kg m^{-2}/10a for RCP4.5 and −2.05 kg m^{-2}/10a for RCP8.5 (Table 3). Figure 7 also shows that the negative trend in SWE gradually begins to level out for RCP2.6, and weakens somewhat for RCP4.5. For RCP8.5, however, SWE continues to decline beyond the end of the 21st century, which agrees with projections of snow cover extent (Zhu and Dong, 2013).

Despite the fact that ensemble simulations show decreasing SWE throughout much of the NH during the three RCPs investigated, we note a significant increasing trend in SWE across Siberia in winter and spring. Nonetheless, owing to the greater geographical extent and magnitude of the projected reductions, there is an overall negative trend in NH SWE during the 21st century.

5 Contribution analysis for SWE change

In both seasonal and zonal contexts, rising temperature plays a fundamental role in projected SWE. Figure 6 shows that the most significant increases in temperature and precipitation occur in winter, but the largest reduction in SWE appears in summer. To identify the relative contributions of temperature and precipitation to changes in SWE, we calculate the partial correlation between SWE and temperature as well as between SWE and

precipitation during the RP, EP, MP and LP for three RCPs (Table 4). SWE has a strong negative partial correlation with temperature and weak correlation with precipitation throughout the 21st century. The negative partial correlation for RCP8.5 decreases from the EP to the LP in the winter half-year, indicating that the rate of the SWE decrease should decline as temperature increases. We also note that the partial correlation between SWE and temperature during the spring uniformly passes the 90% significance test during the EP, MP and LP for RCP8.5, resulting in a persistent decline in springtime SWE, despite the increase in precipitation.

Relative to 1986–2005, the largest absolute decline in simulated SWE also occurs in spring, indicating that the decrease in SWE is related to earlier temperature-driven snowmelt. This result agrees with Räisänen (2008) who proposed that changes in snow conditions would likely depend on present-day temperature. With the increasing temperature, the sensitivity of SWE to temperature averaged over the NH gradually increases from the EP to the LP for the same RCP (not shown).

Temperature increase may change the water cycle and rain–snow ratio (fraction of solid precipitation), and will act to increase the rate of snow melt (fraction of accumulated snowfall). Actually, as shown by Equation 4, SWE can be affected by changes in total precipitation, the fraction of precipitation that falls as snow and the fraction of accumulated snowfall that has not melted. Räisänen (2008) used CMIP3 model simulations to analyze the contributions of the above factors to SWE in Finland and eastern Siberia, and suggested that the major contributor to the change in SWE varies regionally. Thus, over the whole NH, how about the effect of total precipitation, snowfall and accumulated snowfall on SWE during the different periods of the 21st century.

Figure 8 shows the contributions of total precipitation, snowfall and accumulated snowfall to the changes in SWE for three RCPs during three periods of 21st century. During the EP, total precipitation shows an increase in all months, but snowfall decreases in all months. This indicates that changes in total precipitation and snowfall have competing effects and lead to an increase

and decrease in SWE, respectively. Because the magnitude of the decrease in snowfall is larger than the increase in total precipitation, the reduction in SWE is attributed to changes in the fraction of precipitation that falls as snow. The contributions of total precipitation, snowfall and accumulated snowfall grow larger with time. During the LP, temperature increases cause the change in accumulated snowfall to be larger than the change in snowfall after May, so that the former becomes the main control on SWE. In general, from August to May in the next year, the change in SWE is generally related to changes in snowfall, but after May increased melting efficiency dominates the change in SWE.

6 Summary and conclusions

We employed 20 CMIP5 climate models to investigate projected changes in SWE for the 21st century under three different RCPs. The results show a decrease in mean annual SWE for all three RCPs over much of the NH landmass relative to the RP. The most significant reductions occur over the TP and North America, while a minor increase occurs over Siberia, however, the overall pattern in the NH is one of declining SWE. The multi-model ensemble suggests that the negative trend in SWE begins to level out or become stable for RCP2.6 and weakens somewhat for RCP4.5, whereas the declining trend continues beyond the end of the 21st century for RCP8.5. The patterns of change in SWE in spring and winter are the same with the mean annual SWE, since both the magnitude and geographic extent of the reduction in SWE are much greater in spring than in winter, the significant reduction in SWE over NH occurs in spring, however, the largest percent change in SWE does not occur in spring, but in summer, and this indicates that the change in SWE is related to baseline SWE.

Changes in SWE are accompanied by increasing temperature and precipitation during the winter half-year. SWE is not simply a function of temperature, but partial correlations between SWE and both temperature and precipitation indicate that decreases in SWE can be primarily attributed to

increasing temperatures. Furthermore, we note that while atmospheric warming occurs primarily during the winter half-year, coincident with the greater increase in precipitation, greater precipitation cannot compensate for increased snowmelt due to rising temperatures.

Projections of mean annual SWE exhibit a declining trend, and the magnitude of the SWE relative decrease is gradually reduced from south to north over NH. Namely, a more significant reduction in mean annual SWE for all three RCPs occurs at low latitudes throughout the 21st century, accompanied by an anticipated warming trend. Annual maximum SWE also has similar features to mean annual SWE, with the largest decrease observed at low latitudes. However, the correlation between mean annual SWE and temperature suggests that a threshold in the relationship between the SWE and temperature would mitigate the persistent decrease in SWE with increasing temperature.

The 21st century temperature increases are projected to have a pronounced effect on rain–snow ratios and snowmelt. Precipitation also shows an increasing trend, however, because the magnitude of the reduction in snowfall is larger than the increase in total precipitation, the decreasing snowfall becomes the major contributor to the reduction in SWE from August to May in the next year during the 21st century. As the temperature increase, efficient snowmelt dominates the change in SWE after May, especially during the LP. Finally, although model projections have increasing uncertainty later in the 21st century, the trends observed in the simulations remain consistent, and increased model error and bias do not appear to affect the conclusions of this study.

Author contributions. C. H. Wang contributed to the idea and conception of this study, analysis of the result and arrangement the framework of the manuscript.

H. X. Shi carried out the analysis of the data and writing the manuscript with the

assistance of C. H. Wang.

Acknowledgments. This work was supported by the National Natural Science Foundation of China (2013CBA01808, 91437217, 41275061). The snow water equivalent data used in this study are from the European Space Agency (ESA) GlobSnow product and CMIP5 model outputs.

References

Brown, R. D., and Mote, P. W. : The response of Northern Hemisphere snow cover to a changing climate. Journal of Climate, 22, 2124-2145, 2009.

Brutel-Vuilmet, C., Ménégoz, and Krinner, G. : An analysis of present and future seasonal Northern Hemisphere land snow cover simulated by CMIP5 coupled climate models. The Cryosphere, 7, 67-80, doi:10.5194/tc-7-67-2013, 2013.

Chen, S. B., Liu, Y. F., Thomas A. Climatic change on the Tibetan Plateau: potential evapotranspiration trends from 1961–2000[J]. Climatic Change, 76, 291-319, 2006.

Falarz, M. : Long-term variability in reconstructed and observed snow cover over the last 100 winter seasons in Cracow and Zakopane (South Poland). Climate Research, 19, 247-256, 2002.

Groisman, P. Y., Knight, R. W., Karl, T. R., Easterling, D. R., Sun, B., and Lawrimore, J. H.: Contemporary changes of the hydrological cycle over the contiguous United States: Trends derived from in situ observations. Journal of Hydrometeorology, 5, 64-85, 2004.

Hancock, S.; Baxter, R.; Evans, J.; Huntley, B. Evaluating global snow water equivalent products for testing land surface models. Remote Sens. Environ, 128, 107–117, 2013.

Hayhoe, K., Cayan, D., Field, C. B., Frumhoff, P. C., Maurer, E. P., Miller, N. L. and Verville, J. H.: Emissions pathways, climate change, and impacts on California. Proceedings of the National Academy of Sciences of the United States of America, 101, 12422-12427, 2004.

Hosaka, M., Nohara, D. and Kitoh, A.: Changes in snow coverage and snow water equivalent due to global warming simulated by a 20 km-mesh global atmospheric model. SOLA, 1, 93-96, doi: 10.2151, 2005.

Ji, Z. M. and Kang, S. C.: Projection of snow cover changes over China under RCPs scenarios. Climate dynamics, 41, 589-600, 2012.

Lemke, P., Ren, J., Alley, R. B., et al. Observations: changes in snow, ice and frozen ground[J]. Titel: Climate change 2007: the physical science basis; summary for policymakers, technical summary and frequently asked questions. Part of the Working Group I contribution to the Fourth Assessment Report of the Intergovernmental Panel

on Climate Change, 2007: 337-383.

Liu, X. X, Chen, B, D. Climatic warming in the Tibetan Plateau during recent decades[J]. International journal of climatology, 20: 1729-1742, 2000.

Maloney, E. D., Camargo, S. J., Chang, E., et al. North American Climate in CMIP5 Experiments: Part III: Assessment of 21st Century Projections[J]. Journal of Climate. 2014, 27: 2230-2270.

Meehl, G. A., Stocker, T. F., Collins, W. D., Friedlingstein, P., Gaye, A.T., Gregory, J. M., Kitoh, A., Knutti, R., Murphy, J. M., Noda, A., Raper, S. C. B., Watterson, I. G., Weaver, A. J., and Zhao, Z. C. : Global Climate Projections. In: Climate Change 2007: The Physical Science Basis. Contribution of Working Group I to the Fourth Assessment Report of the Intergovernmental Panel on Climate Change [Solomon, S.,D. Qin, M. Manning, Z. Chen, M. Marquis, K.B. Averyt, M. Tignor and H.L. Miller (eds.)]. Cambridge University Press, Cambridge, United Kingdom and New York, NY, USA, pp, 772, 2007.

Mote, P. W.: Climate-Driven Variability and Trends in Mountain Snowpack in Western North America. Journal of Climate, 19, 6209-6220, 2006.

Mote, P. W., Hamlet, A. F., Clark, M. P. and Lettenmaier, D. P. : Declining mountain snowpack in western North America. Bulletin of the American Meteorological Society, 86, 39-49, 2005.

Pierce, D. W., et al. Attribution of declining Western U.S. snowpack to human effects[J. Journal of Climate. 21, 6425–6444, 2008.

Räisänen, J. : Warmer climate: less or more snow? Climate Dynamics, 30, 307-319, 2008.

Räisänen, J. and Eklund, J. : 21st Century changes in snow climate in Northern Europe: a high-resolution view from ENSEMBLES regional climate models. Climate Dynamics, 38 : 2575–2591, doi:10.1007/s00382-011-1076-3, 2012.

Scherrer, S. C., Appenzeller, C. and Laternser, M. : Trends in Swiss alpine snow days—the role of local and large scale climate variability. Geophysical Research Letters, 31, L13215, doi:10.1029/2004GL020255, 2004.

Stewart, I. T., Cayan, D. R. and Dettinger, M. D. : Changes towards earlier streamflow timing across western North American. Journal of climate, 18, 1136-1155, 2005.

Stocker, T. F., Qin, D. H., Plattner, G. K., Tignor, M., Allen, S. K., Boschung, J., Nauels, A., Xia, Y., Bex, V., and Midgle, P. M. : Summary for Policymakers. In: Climate change 2013: The Physical Scientific Basis. Contribution of Working Group I to the Fifth Assessment Report of the Intergovernmental Panel on Climate Change. Cambridge University Press, Cambridge, United Kingdom and New York, NY, USA, pp, 4, 2013.

Takala, M.; Luojus, K.; Pulliainen, J.; Derksen, C.; Lemmetyinen, J.; Kärnä, J.P.; Koskinen, J.; Bojkov, B. Estimating northern hemisphere snow water equivalent for climate research through assimilation of space-borne radiometer data and ground-based measurements. Remote Sens. Environ. 115, 3517–3529, 2011.

Vavrus, S. : The role of terrestrial snow cover in the climate system. Climate dynamics, 29, 73-88, 2007.

Vojtek, M., Faško, P. and Šťastný, P. : Some selected snow climate trends in Slovakia with respect to altitude. Acta Meteorologica Universitatis Comenianae, 32, 17-27, 2003.

Wang, C. H., Li, J. and Xu, X. G. University of Quasi-3-year period of temperature in last 50 years and change in next 20 year in China[J]. Plateau Meteorology, 31: 126-136, 2012.

Wang, Z. L. and Wang, C.H. : Predicting the snow water equivalent over China in the next 40 years based on climate models from IPCC AR4. Journal of glaciology and geocryology, 34:1273-1283, 2012.

Zhu, X. and Dong, W. J. : Evaluation and projection of Northern Hemisphere March-April snow cover area simulated by CMIP5 coupled climate models. Progressus Inquisitiones DE Mutatione Climatis, 9(3): 173-180, 2013.

Table 1. Models used in this study.

Number	Model	Institution	Resolution
1	BCC-CSM1-1	Beijing Climate Center, China	2.8° ×2.8°
2	BCC-CSM1-1(m)	Beijing Climate Center, China	1.3° ×1.1°
3	CanESM2	Canadian Center for Climate Modeling and Analysis, Canada	2.8° ×2.8°
4	CCSM4	National Center for Atmospheric Research, USA	1.25° ×0.94°
5	CNRM-CM5	Centre National de RecherchesMeteorologiques / Centre Europeen de Recherche et Formation AvanceesenCalculScientifique	1.4° ×1.4°
6	CSIRO-Mk3-6-0	CSIRO Atmospheric Research, Australia	1.875° 1.875°
7	FGOALS-g2	Chinese Academy of Sciences	1.4° ×6°
8	FIO-ESM	The First Institute of Oceanography, SOA, China	2.8° ×2.8°
9	GFDL-ESM2G	Geophysical Fluid Dynamics Laboratory, USA	2.5° ×2.0°
10	GISS-E2-H	ASA Goddard Institute for Space Studies, USA	2.5° ×2.0°
11	GISS-E2-R	NASA Goddard Institute for Space Studies, USA	2.5° ×2.0°
12	HadCEM2-ES	Met Office Hadley Centre, UK	1.875° × 1.25°
13	MIROC5	Atmosphere and Ocean Research Institute, Japan	1.4° ×1.4°
14	MIROC-ESM-CHEM	Japan Agency for Marine-Earth Science and Technology, Atmosphere and Ocean Research Institute, Japan	2.8° ×2.8°
15	MIROC-ESM	Japan Agency for Marine-Earth Science and Technology, Atmosphere and Ocean Research Institute, Japan	2.8° ×2.8°
16	MPI-ESM-LR	Max Planck Institute for Meteorology, Germany	1.9° ×1.9°
17	MPI-ESM-MR	Max Planck Institute for Meteorology, Germany	1.875° × 1.875°
18	MRI-CGCM3	Meteorological Research Institute, Japan	1.1° ×1.1°
19	NorESM1-ME	Norwegian Climate Center, Norway	2.5° ×1.875°
20	NorESM1-M	Norwegian Climate Center, Norway	2.5° ×1.875°

Table 2. Zonal slope (Slop) of the regression of mean annual SWE and temperature, and correlation coefficients (Cor.) for mean annual SWE and temperature for three RCPs. RP, EP, MP, and LP represent the periods 1986−2005, 2016−2035, 2046−2065, and 2080−2099, respectively.

			RCP2.6			RCP4.5			RCP8.5		
Lat(°N)		RP	EP	MP	LP	EP	MP	LP	EP	MP	LP
20-30	Slop	-0.43*	-0.22	-1.45	-0.36	-0.52*	-0.25	-0.08	-0.23*	-0.23*	-0.08
	Cor.	-0.55*	-0.22	-0.42*	-0.14	-0.69*	-0.34	-0.03	-0.45*	-0.48*	-0.30
30-40	Slop	-2.15*	-4.38*	-0.74	-1.02	-3.39*	-0.85	-2.86	-3.14*	-1.64*	-0.81*
	Cor.	-0.64*	-0.91*	-0.13	-0.13	-0.77*	-0.29	-0.25	-0.84*	-0.78*	-0.68*
40-50	Slop	-1.00*	-0.84	-1.60	-2.97*	-1.69*	-1.06*	-3.02*	-1.77*	-0.89*	-0.76*
	Cor.	-0.62*	-0.44*	-0.39	-0.55*	-0.80*	-0.48*	-0.71*	-0.86*	-0.74*	-0.82*
50-60	Slop	-3.27*	-3.82*	-0.39	-2.68	-3.28*	-3.24*	-2.62*	-3.25*	-2.55*	-1.33*
	Cor.	-0.71*	-0.64*	-0.08	-0.28	-0.75*	-0.65*	-0.57*	-0.80*	-0.78*	-0.67*
60-70	Slop	-2.87*	-2.57*	-2.84	-3.64	-3.67*	-5.10*	-3.71	-4.10*	-3.70*	-2.84*
	Cor.	-0.66*	-0.47*	-0.32	-0.33	-0.74*	-0.76*	-0.35	-0.71*	-0.83*	-0.73*
70-80	Slop	-10.2*	-16.9*	-0.30	-2.40	-4.57*	-5.23*	-2.10	-8.31*	-6.16*	-4.62*
	Cor.	-0.88*	-0.72*	-0.02	-0.35	-0.65*	-0.81*	-0.06	-0.84*	-0.91*	-0.88*

Note: *values exceed the 95% significance test.

Table 3. Trends in SWE over Northern Hemisphere land during 2006−2099 derived from the three RCPs. All trends are significant at 95% confidence level (Mann–Kendall test).

Trend ($kg\ m^{-2}/10a$)	RCPs		
	RCP2.6	RCP4.5	RCP8.5
Autumn	-0.51	-1.17	-1.83
Winter	-0.54	-1.18	-2.18
Spring	-0.61	-1.32	-2.39
Summer	-0.50	-1.09	-1.79
Mean	-0.54	-1.09	-2.05

Table 4. Partial correlations between mean annual SWE and both mean temperature (T) and precipitation (P) over Northern Hemisphere land for three RCPs. RP, EP, MP, and LP represent the periods 1986−2005, 2016−2035, 2046−2065, and 2080−2099, respectively.

			RCP2.6			RCP4.5			RCP8.5		
Month		RP	EP	MP	LP	EP	MP	LP	EP	MP	LP
Jan	T	-0.29	-0.59*	-0.25	-0.1	-0.54*	-0.44*	-0.52*	-0.45*	-0.38*	-0.31
	P	-0.13	-0.22	-0.05	-0.13	0.1	0	-0.14	0.05	-0.05	-0.05
Feb	T	-0.42*	-0.2	-0.1	-0.37*	-0.25	-0.76*	-0.38*	-0.51*	-0.39*	-0.28
	P	0.05	-0.17	-0.11	0.04	-0.11	0.18	0.09	0.02	-0.05	-0.11
Mar	T	-0.22	-0.26	-0.24	-0.54*	-0.42*	-0.17	-0.56*	-0.4*	-0.4*	-0.4*
	P	-0.07	-0.03	-0.09	0.22	-0.05	-0.18	0.05	-0.02	-0.03	0.01
Apr	T	-0.38*	-0.31	-0.14	-0.38*	-0.37*	-0.49*	-0.51*	-0.49*	-0.38*	-0.38*
	P	-0.06	-0.1	0.02	-0.01	-0.09	0.09	0.09	0.11	-0.08	-0.05
May	T	-0.36*	-0.33	-0.31	-0.34	-0.31	-0.46*	-0.5*	-0.48*	-0.42*	-0.41*
	P	-0.07	-0.1	-0.38	-0.06	-0.2	0.07	0.09	0.1	-0.06	-0.01
Jun	T	-0.43*	-0.33	-0.57*	-0.07	-0.26	-0.46*	-0.08	-0.45*	-0.39*	-0.38*
	P	-0.07	-0.09	0.12	-0.06	-0.11	0.11	-0.27	-0.04	0.02	-0.05
Jul	T	-0.48*	-0.48*	0.27	-0.26	-0.56*	-0.54*	-0.51*	-0.04	-0.46*	-0.24
	P	-0.11	0	-0.2	-0.14	-0.08	-0.02	0.05	0.02	-0.09	-0.02
Aug	T	-0.33	-0.48*	-0.36*	-0.21	-0.48*	-0.38*	-0.29	-0.47*	-0.48*	-0.4*
	P	-0.07	-0.25	-0.06	-0.03	0	0	-0.02	-0.18	0	-0.06
Sep	T	-0.35	-0.44*	-0.39*	0.13	-0.3	-0.1	-0.59*	-0.27	-0.24	-0.34
	P	-0.05	-0.13	-0.01	-0.14	-0.17	-0.07	0.14	-0.07	-0.15	-0.04
Oct	T	-0.35	-0.53*	0.18	0.16	-0.47*	-0.21	-0.5*	-0.33	-0.28	-0.25
	P	-0.08	0	-0.09	-0.52	-0.03	0.06	0.07	-0.1	-0.06	-0.06
Nov	T	-0.43*	-0.36*	-0.07	0.01	-0.53*	-0.47*	-0.21	-0.29	-0.21	-0.33
	P	-0.05	-0.11	-0.09	-0.28	0.15	-0.05	-0.2	-0.03	-0.17	0
Dec	T	-0.25	-0.5*	-0.12	0.08	-0.27	-0.58*	-0.35	-0.34	-0.28	-0.28
	P	-0.12	-0.05	-0.01	-0.29	-0.16	-0.05	-0.19	-0.03	-0.05	0.04

Note: *values exceed the 95% significance test.

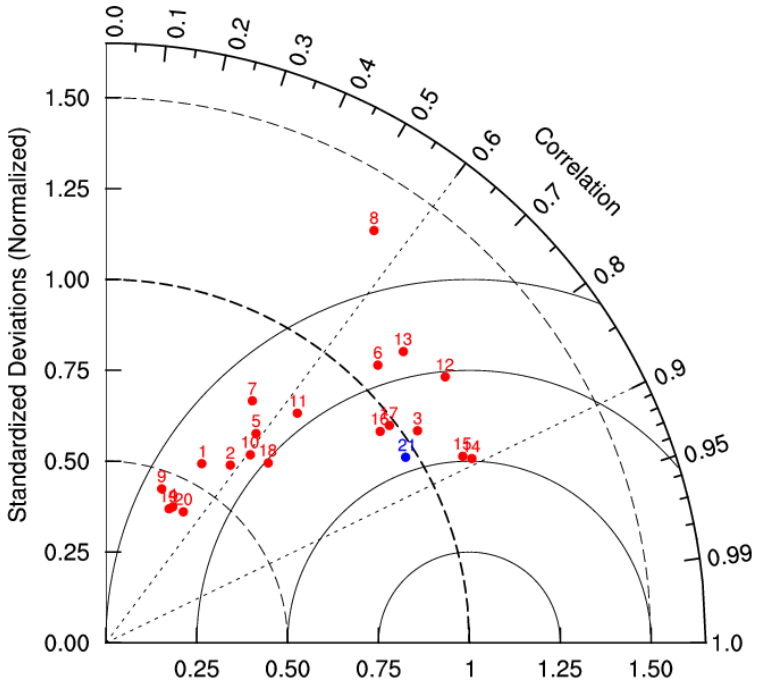

Figure 1. Spatial correlation and standard variance ratios between observed and simulated winter (DJF) mean SWE during 1980–2005. The numbers 1–20 refer to the model names in Table 1. The number 21 indicates the multi-model ensemble. The vertical axis indicates the standard deviation ratios, and the numbers along the arc are the spatial correlation.

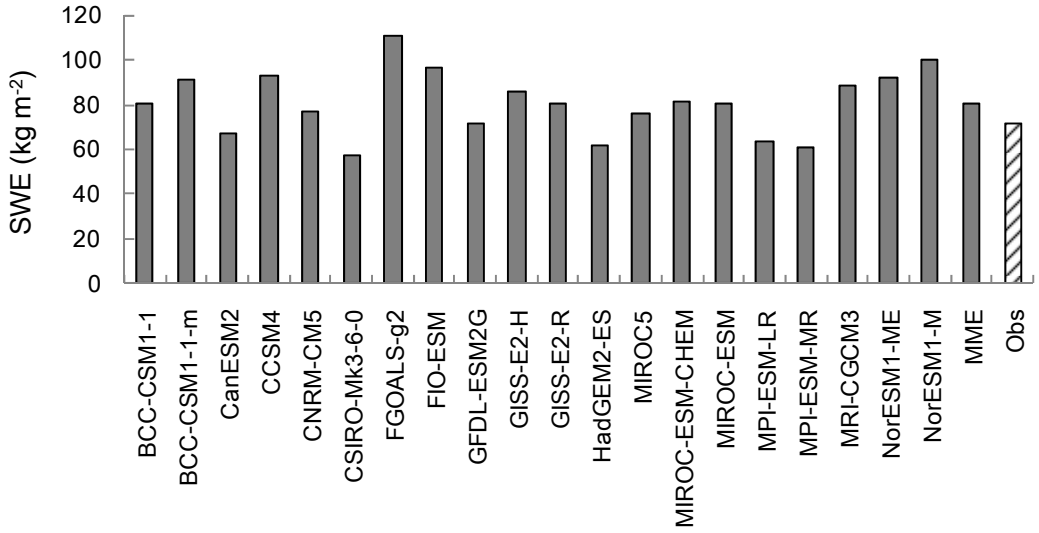

Figure 2. The average of the observed and simulated winter (DJF) mean SWE over Northern Hemisphere land during 1980–2005. The multi-model ensemble (MME) refers to a combination of the 20 models listed in Figure 1.

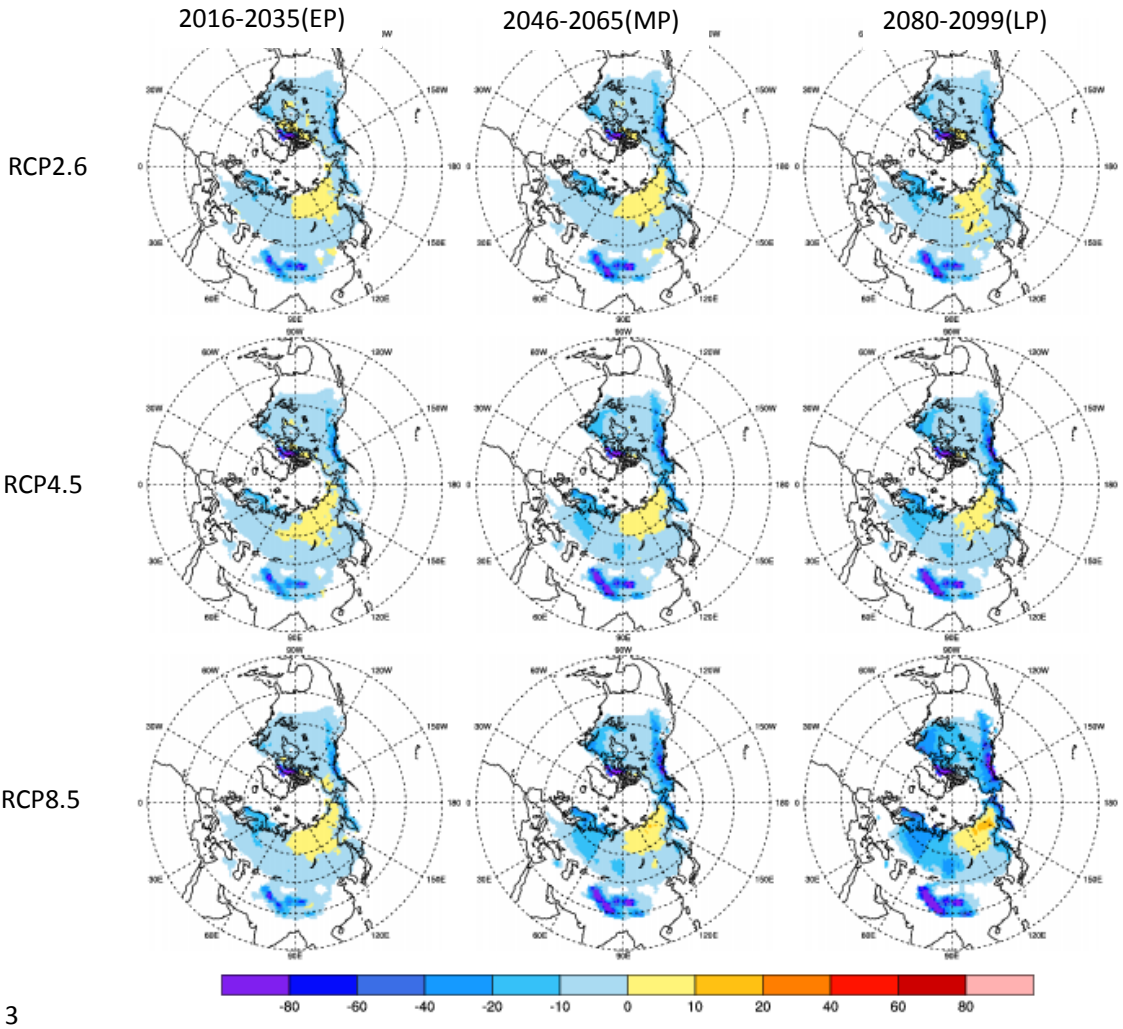

Figure 3. Relative changes in mean annual SWE (%) projected by the CMIP5 ensemble, relative to the 1986−2005 reference period.

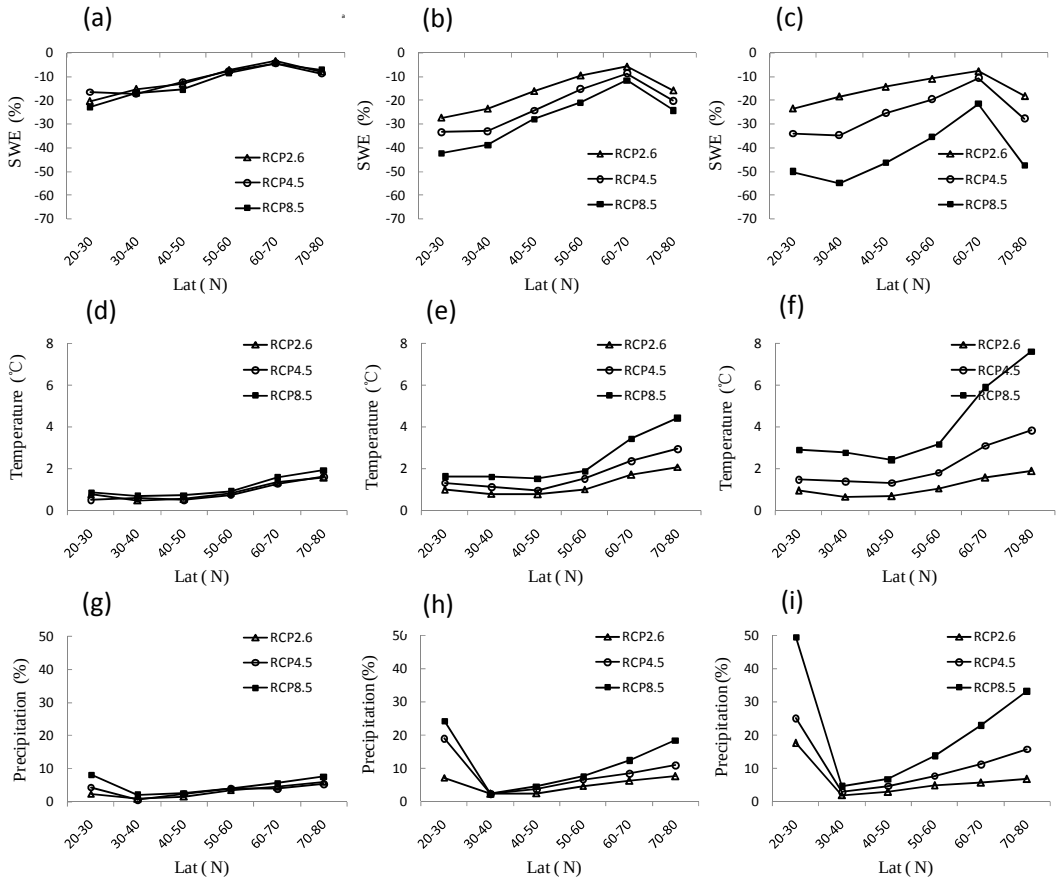

Figure 4. Relative zonal changes in mean annual SWE (a–c), mean annual air temperature (d–f) and mean annual precipitation (g–i) over Northern Hemisphere land for 2016−2035 (left), 2046−2065 (middle), and 2080−2099 (right) relative to the 1986−2005 reference period.

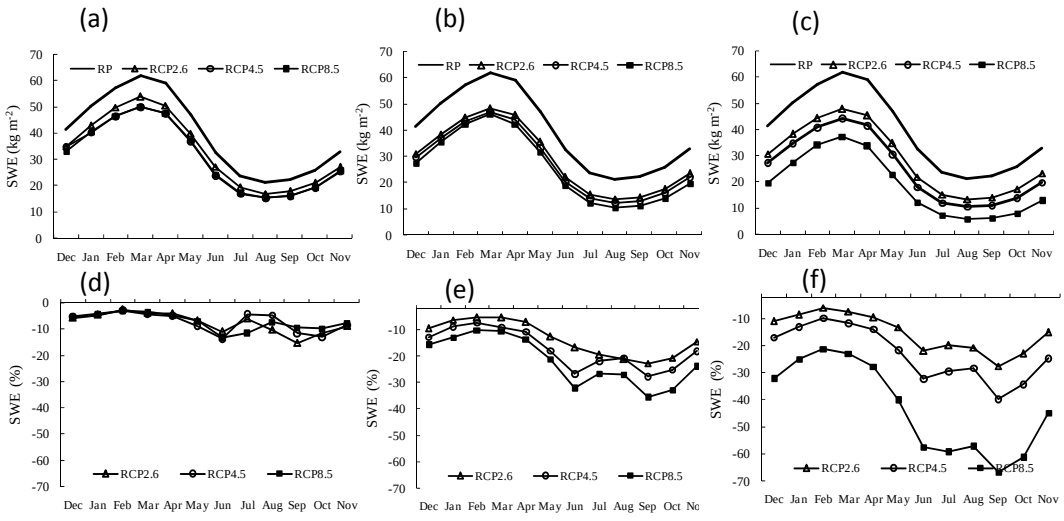

Figure 5. Projected monthly average (a–c) and relative change (RE) (d–f) in SWE over Northern Hemisphere land for 2016−2035 (left), 2046−2065 (middle), and 2080−2099 (right). Panels d–f show changes relative to the 1986−2005 reference period.

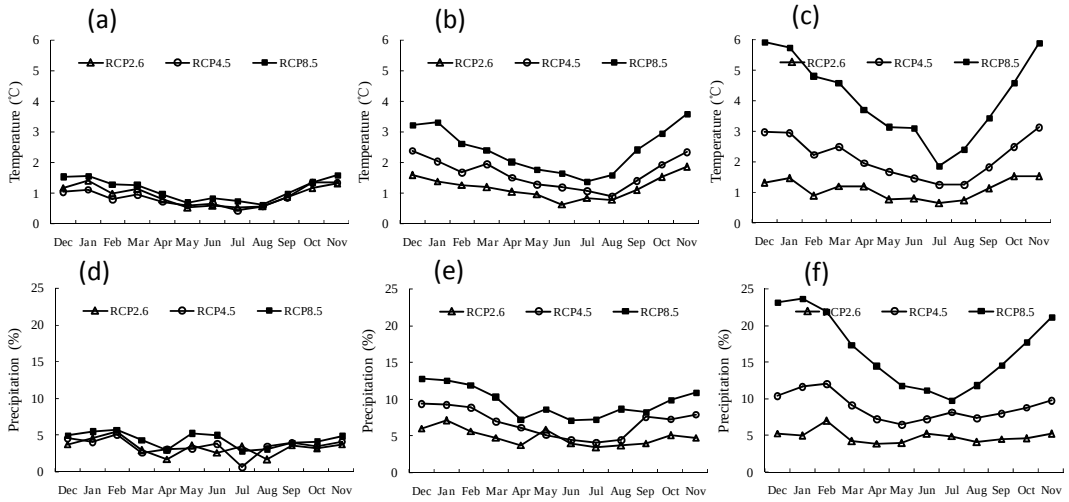

Figure 6. Changes in mean annual air temperature (a–c) and the relative change (RE) in precipitation (d–f) over Northern Hemisphere land for 2016−2035 (left), 2046−2065 (middle), and 2080−2099 (right) for three RCPs, relative to the 1986−2005 reference period.

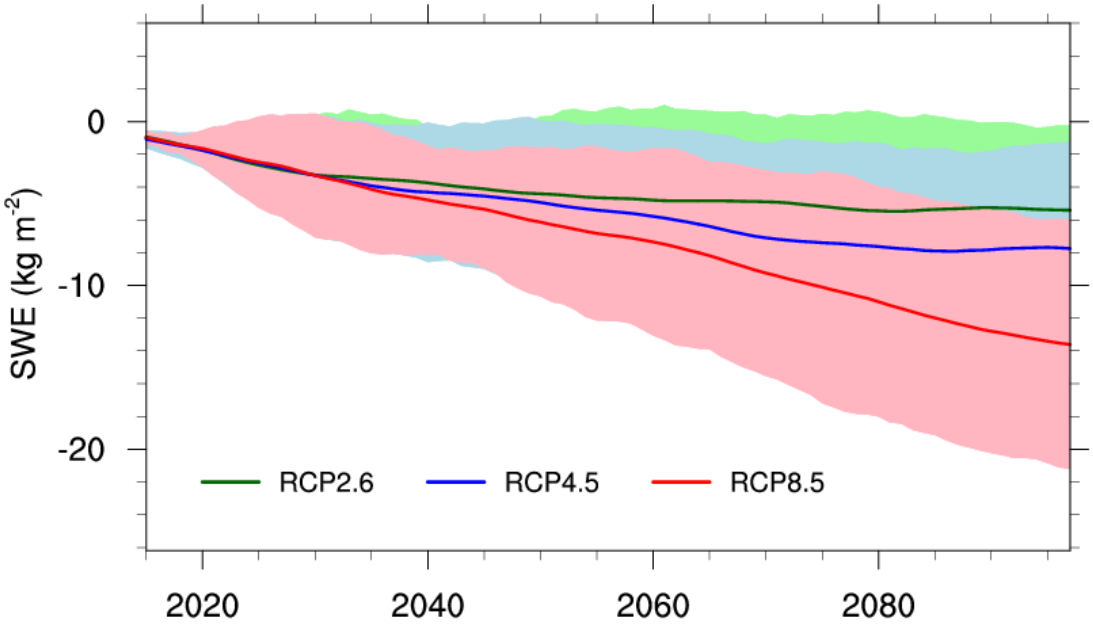

Figure 7. Projected changes in mean annual SWE over Northern Hemisphere land during the 21st century for all three RCPs (green: RCP2.6; blue: RCP4.5; red: RCP8.5). The mean value for the 1986–2005 reference period is subtracted from all values. Also shown is the multi-model mean for all available models for each scenario. The 10-yr running average was derived for each model before calculating the multi-model mean. Shaded areas denote the inter-model standard deviation for each ensemble mean.

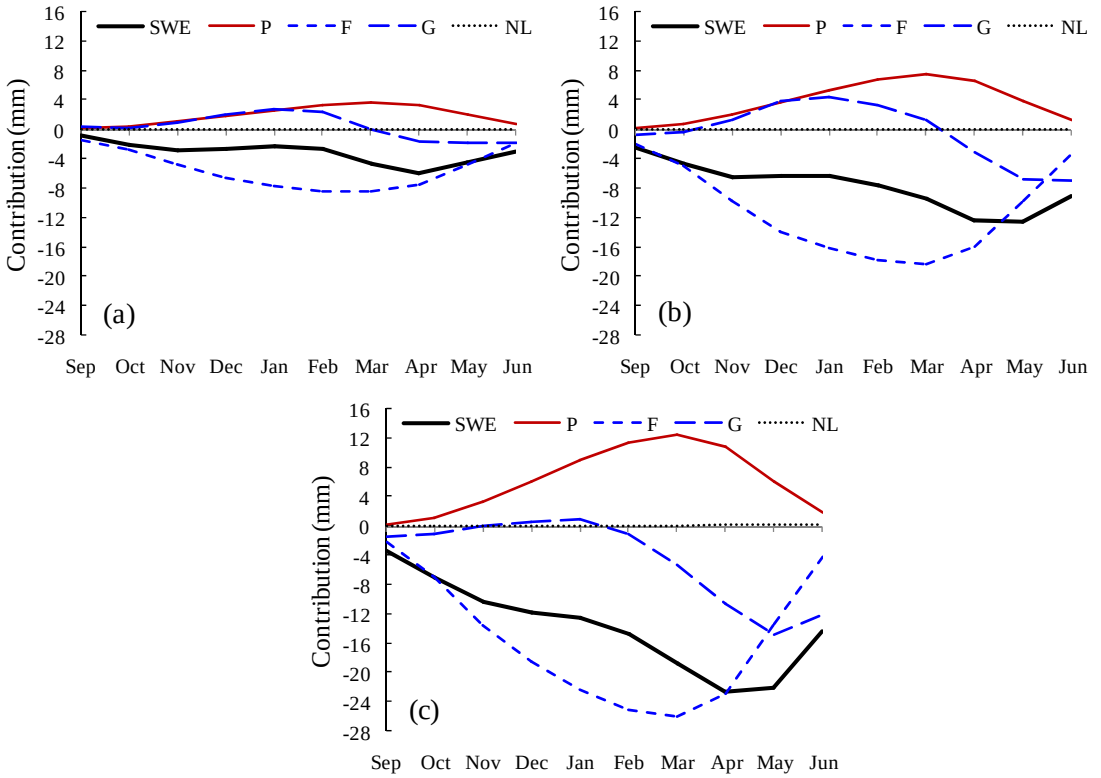

Figure 8. Mean changes in SWE decomposed using Equation (4) to show the contribution of changes in precipitation (ΔP), the fraction of solid precipitation (ΔF), the fraction of accumulated snowfall that remains on the ground (ΔG), and nonlinear terms (*NL*) during the period of 2016-2035 (a), 2046-2065 (b), and 2080-2099 (c) for RCP8.5, relative to the 1986–2005 reference period.